Force characterization and analysis of thin film actuators for untethered microdevices

Federico Ongaro,[1, a)] Qianru Jin,[2] Ugo Siciliani de Cumis,[1] Arijit Ghosh,[2] Alper Denasi,[3] David H. Gracias,[2, 4] and Sarthak Misra[1, 3, b)]

[1)] *Surgical Robotics Laboratory, Department of Biomechanical Engineering, University of Twente, Enschede, 7522 NB, The Netherlands.*

[2)] *Department of Chemical and Biomolecular Engineering, The Johns Hopkins University, Baltimore, MD 21218, USA.*

[3)] *Surgical Robotics Laboratory, Department of Biomedical Engineering, University of Groningen and University Medical Centre Groningen, Groningen, 9713 GZ, The Netherlands.*

[4)] *Department of Materials Science and Engineering, The Johns Hopkins University, Baltimore, MD 21218, USA.*

(Dated: May 6, 2019)

In recent years, untethered microdevices have drawn significant attention due to their small size, weight and their ability to exert forces without the need for wires or tethers. Such microdevices are relevant to implantable biomedical devices, miniature robotics, minimally invasive surgery, and microelectromechanical systems. While devices using these actuators have been widely utilized in pick-and-place and biopsy applications, the forces exerted by these actuators have yet to be characterized and analyzed. Lack of precise force measurements and validated models impedes the clinical applicability and safety of such thin film microsurgical devices. Furthermore, present-day design of thin film microdevices for targeted applications requires an iterative trial-and-error process. In order to address these issues, we present a novel technique to measure the force output of thin film microactuators. Also, we develop and fabricate three designs of residual stress microactuators and use them to validate this technique, and establish a relationship between performance and design parameters. In particular, we find an inverse dependence of the thickness of the actuator and its force output, with 70 nm, 115 nm and 200 nm actuators exerting 7.8 μN, 4.7 μN, and 2.7 μN, respectively. Besides these findings, we anticipate that this microsystem measurement approach could be used for force measurements on alternate microactuators including shape memory, piezo and electromagnetic actuators.

Keywords: Robotics, MEMS, biomedical engineering, nanofabrication

Microscale devices have the potential of revolutionizing the fields of implantable biomedical devices, miniature robotics, minimally invasive surgery, and microelectromechanical systems[1–4]. In recent years, studies have shown these devices operating in hard-to-reach or constrained environments to perform a wide variety of tasks. In particular, they appear to be highly effective for applications such as targeted drug delivery, particle separation, mixing, pumping, assembly, manipulation, microsurgery, chemical analysis, and many more[5–12].

Due to miniaturization requirements, these microdevices cannot use traditional wired actuators, whose onboard power sources cannot be miniaturized to the prescribed scale. In addition, parallel or swarm operations could benefit from unwired actuators that could be mass produced and respond in parallel to an environmental or external stimulus. Consequently, researchers have investigated the development of microactuators capable of wirelessly harnessing power stored within the material itself or from their surroundings[13–16].

In particular, thin film microactuators are drawing significant attention for such tasks[17–19]. These actuators are developed combining thin-film deposition techniques with actuation principles such as magnetostriction, inverse piezoelectricity, shape memory effect and bimetallic stress mismatches. Consequently, thin film actuators can be triggered using a variety of signals, including magnetic fields, electric fields, or temperature changes[20,21]. This actuation flexibility is combined with a number of properties, such as high power to weight ratios, ease of fabrication, wireless actuation, large transformation stresses, chemical resistance, and biocompatibility, that render thin film actuators particularly suitable for untethered microdevices for biomedical applications[22–24].

In biomedical and clinical applications, reliable microactuators would have to operate with high predictability and repeatability, in order to ensure that they do not pose any risk of damage to the manipulated material. While finite element (FE) analyses and force measurements have been previously presented for piezoelectric, electromagnetic, and shape memory microactuators, the force exerted by untethered bimetallic microactuators has yet to be measured[25–41]. Consequently, microscale adaptations of macroscale models have to be used for the estimation of the force output of such actuators. However, with scale changes of several orders of magnitude, previously negligible effects can become exceptionally relevant. Clearly, FE methods do address some of these

[a)] Electronic mail: f.ongaro@utwente.nl

[b)] Electronic mail: s.misra@utwente.nl.

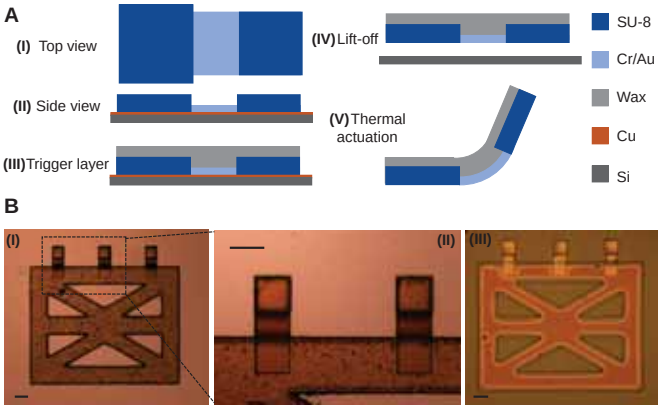

Figure 1. (A) Fabrication schematics. (I) Top view, and (II) sideview of residual stress powered thin film bilayer actuators fabricated on a copper sacrificial layer on a silicon substrate; (III) addition of a thermosensitive trigger layer made of wax or photoresist enables stimuli responsive release of stress and actuation; (IV) actuator lift-off by dissolution of a copper sacrificial layer; (V) actuator folding by thermal actuation of the trigger layer. (B) (I) Representative example of an actuator holder with 3 attached actuators; (II) zoom-in image of the actuators; (III) image of the lift-off process showing the copper dissolution process underneath the actuator. Scale bar in B (I-III) represents 200 μm.

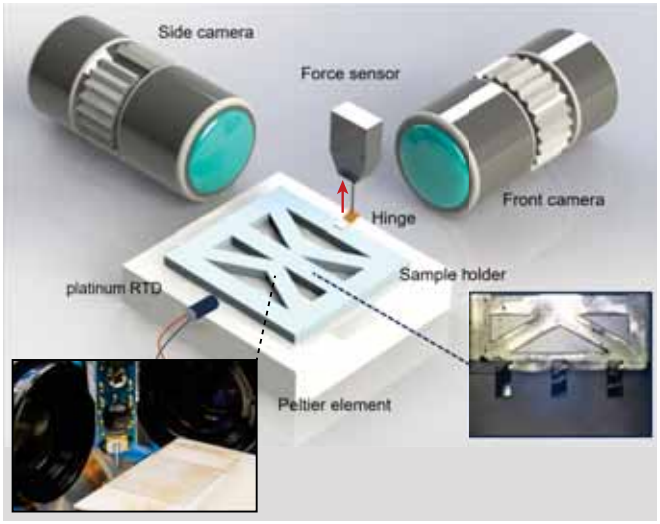

Figure 2. Optical image and computer assisted rendering of the used setup. Two CCD cameras combined with zoom modules are used for orthogonal imaging of the sample. The force sensor is mounted on a vertical linear-stage and is free to move only in the z direction. The system is capable of measuring compressive forces in the range of -100 μN to 100 μN along the probe axis (red arrow), with a resolution of 100 nN. In order to minimize spurious signals a low-noise power supply is combined with an integrated voltage regulator. A temperature closed-loop control is implemented on a microcontroller. The temperature is increased using a Peltier element, while an amplified RTD sensor signal is used for feedback. Finally, an XYZ stage (not shown) is used for sample positioning with μm precision. Further details are provided in Table I.

effects, nonetheless the reliability of the resulting model cannot be guaranteed until it is validated. In turn, the unreliability of such models impedes the evaluation of the clinical safety and applicability of thin film devices in microsurgical environments. Moreover, the absence of precise force estimates constrain micro-device designers to perform time-consuming trial-and-error procedures.

The reason behind this lacuna is that the measurement of forces at this scale is challenging. Not only does it require precise sensors, but also micron-precision positioning and pose reconstruction techniques. These latter techniques are indispensable to perform accurate measurements, especially for rotary actuators, for which measured forces are stricly related to the length of the arm.

In this study, we use a stereo microscopy system, a calibrated force sensor, and a closed-loop thermocontroller to develop a reliable technique to measure the force output of thin film microactuators. Further, we design and fabricate three thin film residual stress powered microactuators, which are used to validate the effectiveness of this technique. Moreover, we take advantage of several designs to analyze the effect of the design parameters on the forces exerted by the microactuators. Finally, an estimation of the forces required in clinical environments is presented. Overall, this work provides quantitative measurements for the analysis of microscale thin film actuators, improving their modeling and design processes.

The thin film actuators presented in this work are fabricated as follows[1,18,43]: first, a sacrificial layer of 15 nm Cr and 200 nm Cu is deposited by thermal evaporation to allow for later actuator lift off. Subsequently, AZ5214 photoresist based lithography is used to pattern the stress bilayer. Then, thin films of 75 nm Cr and the desired thickness of Au are deposited by thermal evaporation. SU-8 3010 is used in the photolithography procedure to create the thick rigid holder and the arm of the actuator (Fig. 1). In the next step, we pattern the thermosensitive trigger layer using wax molded in a 10 um thick mold of SPR220 photoresist. The structures can then be released from the substrate using a copper etchant (APS-100) to dissolve the copper sacrificial layer. Finally, the actuators are ready to be tested after being thoroughly rinsed in DI water.

The force exerted by these actuators is measured in the setup shown in Figure 2, while a detailed list of the used components is reported in Table I. Similar to previous literature, two micromanipulators are used to align the actuator and the sensor, while positioning them at a distance of 5 μm[38]. Two orthogonally-oriented cameras are used to inspect this alignment and ensure correct positioning in three dimensions[42]. The calibrated nano-force sensor can then measure the contact forces as the closed-loop temperature controller triggers the actuation of the thin film actuator (Fig. 3). For this purpose, the temperature controller is regulated to reach the reference temperature of 40° C, 3° C above the melting temperature

of the wax used to constrain the microactuators. As the actuation is driven by the release of residual stress, the direction of motion of these actuators cannot be reversed.

Throughout the experiments we analyze the effect of changes in the thickness of the Au layer on the force exerted by the thin-film actuators. For this purpose, the actuators are positioned on top of a slide of hydrolytic class 1 borosilicate glass (170 μm thick) that is placed on a Peltier heating element (initially at room temperature). After the sample is correctly positioned using the XYZ linear stage, the closed-loop temperature control is activated, reaching the reference temperature of 40° C in about 25 s. In turn, this temperature softens the wax layer, allowing the microactuator to release its stress. However, constrained by the force sensor, the hinge of microactuator is not able to fold, consequently exerting its force on the tip of the sensor (Fig. 3). A few minutes after the force output stabilizes, the experiment is terminated. Ten trials are performed for each of the three selected residual-stress layer thicknesses: 70 nm, 115 nm, and 200 nm (Fig. 4).

The measured data shows that the force decreases with increasing thickness of the bilayer (Table II). In particular, as the Au thickness increases from 70 nm to 115 nm, and from 115 nm to 200 nm, we notice a 39% and 43% force decrease, respectively. Here, it may be noted that the Au layer acts as a support to the active Cr film, that provides the actuating force. Thus changing the thickness of Au in the stress bilayer, by keeping the Cr thickness constant, we look only at the dependence of the force on the thickness of the bilayer. Consequently, the reduction in the force with increasing bilayer thickness can be linked to the multilayer thin film curvature model, which predicts that by changing the thickness of the passive layer, the folding angle is decreased due to the increased bending rigidity of the film[44–46]. We hypothesize that the folding angle should have a direct correlation with the force for a fixed length of the hinge of the actuator. Moreover, we also notice differences in the behavior of the actuators. Specifically, thinner actuators exhibit a higher variability of the force output and its derivative than thicker ones (Table II). We believe these phenomena to be due to lower structural integrity and larger variability in deposition of thinner films.

In recent years, thin film bilayer actuators have been increasingly proposed for the actuation of untethered sur-

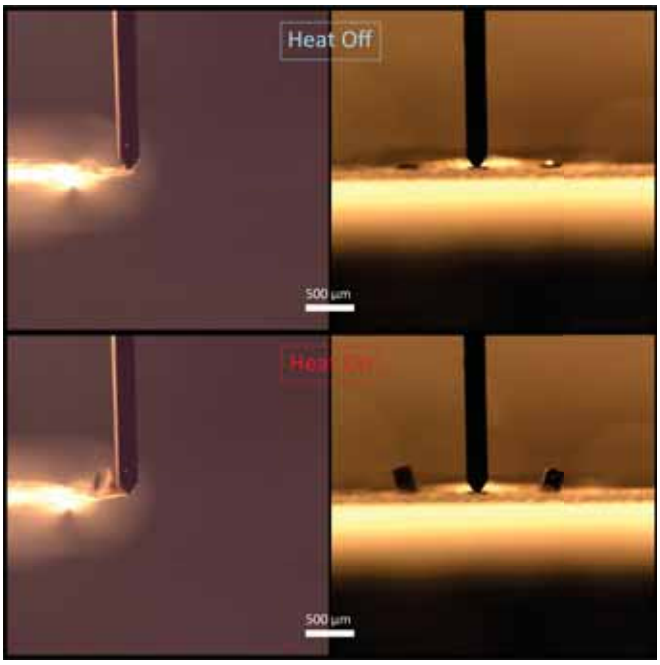

Figure 3. Representative microscopic images of front (right) and side (left) views of the actuators during a force measurement experiment. At the beginning of the experiment, the force actuator is positioned at less than 5 μm distance from the end of one tip of the actuator, as shown in the top images. The temperature reference is then set to 40°C. As the temperature increases the wax layer softens, allowing the release of the unconstrained stress of the bilayer. Consequently, the actuator will start folding until it comes in contact with the force sensor, providing a measurement of its force output. Not being constrained by the force sensor, the other actuators on the sample will continue to fold as shown in the bottom images. Scale bar: 500 μm.

Table I. This table lists the components used for the assembly of the system. We refer the reader to previous publications for details regarding the design of the support structure[42].

Component	**Model**
Cameras	Grasshopper 3 *(FLIR, USA)*
Optics	1.7-12× Zoom Module *(Qioptiq, UK)*
Force Sensor	FT-S100 *(FemtoTools, Switzerland)*
Power Supplier	SM 70-22 *(Delta Elektronika, Netherlands)*
Heater	180 W Peltier Element *(Farnell, Netherlands)*
Temperature Sensor	Pt 1 kΩ RTD *(RS, Netherlands)*
Amplifier	MAX31865 *(Adafruit, USA)*
Microcontroller	Arduino Uno *(Arduino, Italy)*
Micromanipulators	XYZ stage *(MISUMI, Japan)*

Table II. Table summarizing the obtained results relating the gold layer thickness to the weight and average maximum force (over ten trials) of the thin film microactuators. The obtained results appear consistent with preliminary FE analyses and previous literature on thin film shape memory alloy microactuators of similar footprint[22].

Au Thickness	**Weight** (μg)	**Max Force** (μN)
70 nm	1.57	7.8±1.1
115 nm	1.68	4.7±0.9
200 nm	1.78	2.7±0.4

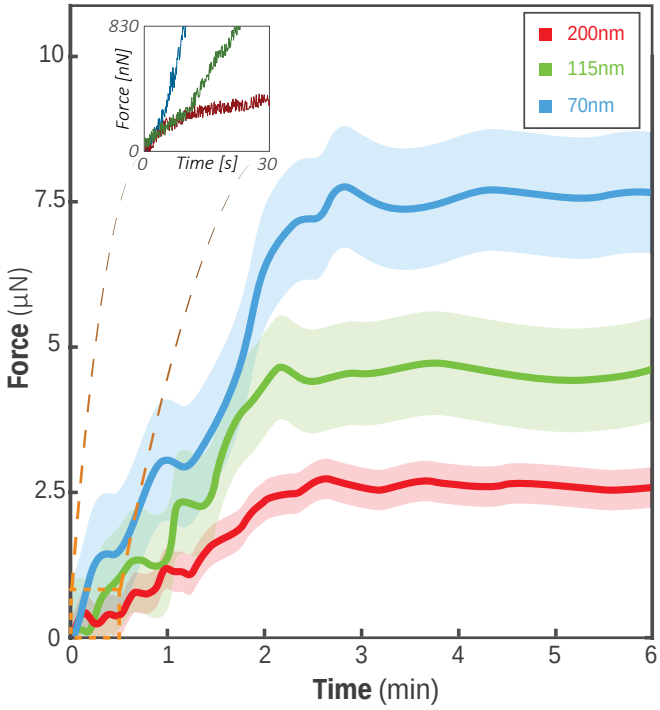

Figure 4. Plot of the force output of the thin film actuators during the experiments. The red, green, and blue curves in the main plot depict the average force output over the ten trials for thin film acutators with Au thickness of 200 nm, 115 nm, and 70 nm, respectively. The similarly-colored shaded area represents the standard deviation. Conversely, the inset shows a representative result of the individual actuators. These raw-data curves are colored in a darker shade of color, in order to distinguish the performance of a single actuator from the average results.

gical microrobots[22–24]. Therefore, it is interesting to compare the measured force to that required in surgical interventions, particularly for piercing soft tissue. However, the quantitative mechanical analyses of soft body penetration are strongly dependent on specific combinations of the perforated material, and shape and material of the perforator. Consequently, a complex *ex-vivo* experimental analysis would be required to exactly model such interactions. In spite of this, several studies model and measure the forces involved in the insertion of microneedles[47–51]. Assuming a similar interaction for our actuators, a pressure of about 76 kPa would be required (using porcine intestine as model). Thus a cylindrical thin film 8 μN actuator having a tip radius smaller than 6 μm could penetrate such tissue. Most thin film actuators, as the ones presented here, have a contact tip that is significantly smaller, yet they do not have a circular cross-section. Therefore, further investigation is required to experimentally determine their clinical applicability based on specific designs.

Overall, in this study we develop a procedure to measure the force output of thin film microactuators. In particular, the experimental validation of such a technique provides the first measurement of the force of wireless bilayer thin film actuators. Moreover, the effect of film thickness is also analyzed, showing a strong relation between force and film thickness. This procedure and data analysis provide crucial tools for the design and validation of microdevices intended to exert forces in a specific range. Finally, this work also provides a preliminary estimation of forces required for the use of microdevices in microsurgical applications.

In the future, we will analyze the effect of other design aspects and quantify the force output of more complicated structures. Moreover, it will be interesting to see how the force estimates obtained from these measurements will translate to soft tissue puncturing experiments using stress driven actuators.

FUNDING INFORMATION

This research has received funding from the European Research Council (ERC) under the European Union's Horizon 2020 Research and Innovation programme (Grant Agreement #638428 - project *ROBOTAR*: Robot-Assisted Flexible Needle Steering for Targeted Delivery of Magnetic Agents). We also acknowledge supprot from the National Science Foundation (CMMI-1635443).

REFERENCES

[1]T. G. Leong, C. L. Randall, B. R. Benson, N. Bassik, G. M. Stern, and D. H. Gracias, Proceedings of the National Academy of Sciences **106**, 703 (2009).
[2]A. Ichikawa, S. Sakuma, M. Sugita, T. Shoda, T. Tamakoshi, S. Akagi, and F. Arai, Journal of Micromechanics and Microengineering **24**, 095004 (2014).
[3]M. Sitti, H. Ceylan, W. Hu, J. Giltinan, M. Turan, S. Yim, and E. Diller, Proceedings of the IEEE **103**, 205 (2015).
[4]D. Rus and M. T. Tolley, Nature Reviews Materials , 1 (2018).
[5]D.-H. Kim, P. K. Wong, J. Park, A. Levchenko, and Y. Sun, Annual review of biomedical engineering **11**, 203 (2009).
[6]A. G. Banerjee, S. Chowdhury, S. K. Gupta, and W. Losert, Journal of Biomedical Optics **16**, 051302 (2011).
[7]S. Martel, IEEE Control Systems **33**, 119 (2013).
[8]S. Chowdhury, W. Jing, and D. J. Cappelleri, Journal of Micro-Bio Robotics **10**, 1 (2015).
[9]S. Lee, S. Kim, S. Kim, J.-Y. Kim, C. Moon, B. J. Nelson, and H. Choi, Advanced Healthcare Materials **7** (2018), 10.1002/adhm.201700985.
[10]Z. Zhang, X. Wang, J. Liu, C. Dai, and Y. Sun, Annual Review of Control, Robotics, and Autonomous Systems (2018).
[11]I. S. Khalil, A. F. Tabak, M. A. Seif, A. Klingner, and M. Sitti, PloS one **13**, e0206456 (2018).
[12]L. N. Pham and J. J. Abbott, in *Proceedings of the IEEE/RSJ International Conference on Intelligent Robots and Systems (IROS)* (2018) pp. 1783–1788.
[13]F. Ongaro, C. Yoon, F. van den Brink, M. Abayazid, S. H. Oh, D. H. Gracias, and S. Misra, in *Proceedings of the IEEE International Conference on Biomedical Robotics and Biomechatronics (BioRob)* (2016) pp. 299–304.
[14]F. Ongaro, S. Scheggi, C. Yoon, F. Van den Brink, S. H. Oh, D. H. Gracias, and S. Misra, Journal of micro-bio robotics **12**, 45 (2017).

[15]Y. Dong, H. R. Holmes, and K. F. Böhringer, Langmuir **33**, 10745 (2017).
[16]J. Zhang and E. Diller, Soft robotics (2018).
[17]E. Gultepe, J. S. Randhawa, S. Kadam, S. Yamanaka, F. M. Selaru, E. J. Shin, A. N. Kalloo, and D. H. Gracias, Advanced Materials **25**, 514 (2013).
[18]F. Ongaro, S. Scheggi, A. Ghosh, A. Denasi, D. H. Gracias, and S. Misra, PloS one **12**, e0187441 (2017).
[19]Q. Yang, H. Park, T. N. Nguyen, J. F. Rhoads, A. Lee, R. T. Bentley, J. W. Judy, and H. Lee, Sensors and Actuators B: Chemical **273**, 1694 (2018).
[20]H. Kueppers, T. Leuerer, U. Schnakenberg, W. Mokwa, M. Hoffmann, T. Schneller, U. Boettger, and R. Waser, Sensors and Actuators A: Physical **97**, 680 (2002).
[21]C. Luo, W. Tai, C.-W. Yang, G. Cao, and I. Shen, Journal of Vibration and Acoustics **138**, 061015 (2016).
[22]P. Krulevitch, A. P. Lee, P. B. Ramsey, J. C. Trevino, J. Hamilton, and M. A. Northrup, Journal of Microelectromechanical Systems **5**, 270 (1996).
[23]W. C. Lee, J. Park, D. A. Weitz, S. Takeuchi, and A. P. Alivisatos, in *Proceedings of the International Conference on Micro Electro Mechanical Systems (MEMS)* (IEEE, 2015) pp. 8–9.
[24]M. Kabla, E. Ben-David, and D. Shilo, Smart Materials and Structures **25** (2016).
[25]W. Fang and J. Wickert, Journal of Micromechanics and Microengineering **6**, 301 (1996).
[26]M. Tanimoto, F. Arai, T. Fukuda, H. Iwata, K. Itoigawa, Y. Gotoh, M. Hashimoto, and M. Negoro, in *Proceedings of the Eleventh Annual International Workshop on Micro Electro Mechanical Systems. An Investigation of Micro Structures, Sensors, Actuators, Machines and Systems* (IEEE, 1998) pp. 504–509.
[27]N. Hasegawa, S. Sakuma, Y. Murozaki, and F. Arai, in *Proceedings of the International Symposium on Micro-NanoMechatronics and Human Science (MHS)* (IEEE, 2017) pp. 1–3.
[28]H. Tobushi, H. Hara, E. Yamada, and S. Hayashi, Smart Materials and Structures **5**, 483 (1996).
[29]P. Muralt, IEEE transactions on ultrasonics, ferroelectrics, and frequency control **47**, 903 (2000).
[30]M. Haque and M. Saif, Sensors and Actuators A: Physical **97**, 239 (2002).
[31]Y. Lai, J. McDonald, M. Kujath, and T. Hubbard, Journal of Micromechanics and Microengineering **14**, 49 (2003).
[32]F. F. Duval, S. A. Wilson, G. Ensell, N. M. Evanno, M. G. Cain, and R. W. Whatmore, Sensors and Actuators A: Physical **133**, 35 (2007).
[33]K. Miyamoto, T. Jomori, K. Sugano, O. Tabata, and T. Tsuchiya, Sensors and Actuators A: Physical **143**, 136 (2008).
[34]O. Araromi, A. Poulin, S. Rosset, M. Favre, M. Giazzon, C. Martin-Olmos, M. Liley, and H. Shea, in *Proceedings of the Electroactive Polymer Actuators and Devices (EAPAD)*, Vol. 9430 (2015).
[35]C. Ma, Y. Chen, J. Chen, and J. Chu, Applied Physics Express **9**, 116601 (2016).
[36]M. Ghidelli, M. Sebastiani, C. Collet, and R. Guillemet, Materials & Design **106**, 436 (2016).
[37]F. Tavakolian, A. Farrokhabadi, and M. Mirzaei, Microsystem Technologies **23**, 839 (2017).
[38]H.-T. Lee, M.-S. Kim, G.-Y. Lee, C.-S. Kim, and S.-H. Ahn, Small **14** (2018).
[39]M. Power, A. J. Thompson, S. Anastasova, and G.-Z. Yang, Small **14** (2018).
[40]L. E. Schultz, T. J. Cogger, R. Good, J. Schneider, R. Rothschild, and W. Nollet, in *Aerodynamic Measurement Technology and Ground Testing Conference* (2018) pp. 37–45.
[41]A. Emiliavaca, C. de Araújo, C. Souto, and A. Ries, Smart Materials and Structures **28**, 10 (2018).
[42]F. Ongaro, S. Pane, S. Scheggi, and S. Misra, IEEE Transactions on Robotics **35**, 174 (2019).
[43]S. Pandey, E. Gultepe, and D. H. Gracias, JoVE (Journal of Visualized Experiments) **72**, e50022 (2013).
[44]G. P. Nikishkov, Journal of Applied Physics **94**, 5333 (2003).
[45]N. Bassik, G. M. Stern, M. Jamal, and D. H. Gracias, Advanced Materials **20**, 4760 (2008).
[46]P. Tyagi, N. Bassik, T. G. Leong, J.-H. Cho, B. R. Benson, and D. H. Gracias, Journal of Microelectromechanical Systems **18**, 784 (2009).
[47]O. A. Shergold and N. A. Fleck, in *Proceedings of the Royal Society of London A: Mathematical, Physical and Engineering Sciences*, Vol. 460 (The Royal Society, 2004) pp. 3037–3058.
[48]M. R. Prausnitz, Advanced drug delivery reviews **56**, 581 (2004).
[49]S. P. Davis, B. J. Landis, Z. H. Adams, M. G. Allen, and M. R. Prausnitz, Journal of biomechanics **37**, 1155 (2004).
[50]X. Kong and C. Wu, Physical Review E **82** (2010).
[51]A. Shademan, R. S. Decker, J. D. Opfermann, S. Leonard, A. Krieger, and P. C. Kim, Science translational medicine **8** (2016).